Chinese Chemical Letters 32 (2021) 1972–1976

Contents lists available at ScienceDirect

Chinese Chemical Letters

journal homepage: www.elsevier.com/locate/cclet

Communication

Screening performance of methane activation over atomically dispersed metal catalysts on defective boron nitride monolayers: A density functional theory study

Xiao-Ming Cao[a,*], Haijin Zhou[a], Liyang Zhao[a], Xuning Chen[a], Peijun Hu[a,b]

[a] Joint International Research Laboratory for Precision Chemistry and Molecular Engineering, Centre for Computational Chemistry and Research Institute of Industrial Catalysis, School of Chemistry and Molecular Engineering, East China University of Science and Technology, Shanghai 200237, China
[b] School of Chemistry and Chemical Engineering, The Queen's University of Belfast, Belfast BT9 5AG, United Kingdom

ARTICLE INFO

Article history:
Received 19 June 2020
Received in revised form 31 July 2020
Accepted 9 September 2020
Available online 10 September 2020

Keywords:
Boron nitride monolayer
Density functional theory
Methane activation
Surface reactive oxygen species
Transition metal center

ABSTRACT

Methane (CH_4) controllable activation is the key process for CH_4 upgrading, which is sensitive to the surface oxygen species. The high thermal conductivity and superb thermal stability of the hexagonal boron nitride (*h*-BN) sheet makes a single transition metal atom doped hexagonal boron nitride monolayer (TM-BN) possible to be a promising material for catalyzing methane partial oxidation. The performances of 24 TM-BNs for CH_4 activation are systematically investigated during the CH_4 oxidation by means of first-principles computation. The calculation results unravel the periodic variation trends for the stability of TM-BN, the adsorption strength and the kind of O_2 species, and the resulting CH_4 activation performance on TM-BNs. The formed peroxide O_2^{2-} of which the O—O bond could be broken and O^- anions are found to be reactive oxygen species for CH_4 activation under the mild conditions. It is found that the redox potential of TM center, including its valence electron number, coordination environment, and the work function of TM-BN, is the underlying reason for the formation of different oxygen species and the resulting activity for CH_4 oxidative dehydrogenation.

The recent surge in natural gas production, fueled by the exploitation of shale gas reserves, is providing an abundant supply of methane. Tapping into this supply and converting methane into the chemicals with higher values can significantly impact the chemical industry. This could add new supplies for raw materials [1,2]. However, methane activation always remains a major challenge. It is difficult to selectively break its strong and localized C–H bond due to the high ionization energy, low electron affinity, and high symmetry [3,4].

Amongst the potential routes for methane upgrading, the favourable thermodynamics enables the oxidation processes to offer the greatest potential [5]. However, the stronger bond energy (440 kJ/mol) compared to its oxygenates [6,7] results in a tremendous challenge to achieve desired partial oxidation products instead of the complete combustion [8–11]. It is of vital importance to understand the reaction mechanisms to pave the way to improve the catalyst. However, its reaction network is rather complex. The different reactive surface oxygen species could be generated during the oxidation, which would trigger a variety of reaction pathways, respectively. Hence, it is indispensable to understand the role of the surface reactive oxygen species in the reaction and how to controllably produce desired reactive surface oxygen species through modulating the electronic structure of the catalyst surface. In general, anion radical $O^{-\bullet}$* (* denotes the surface intermediates throughout the paper), superoxide $O^{2-\bullet}$*, and peroxide O_2^{2-}* are the surface oxygen species most commonly implicated in methane activation chemistry [12,13]. A great amount of work has revealed that the H could be abstracted from the methane by $O^{-\bullet}$*, $O^{2-\bullet}$* or O_2^{2-}* on the catalyst surface. The anionic $O^{-\bullet}$* anion was regarded as the possible most active surface oxygen over the La_2O_3 surface [14]. The peroxide O_2^{2-}* anion was also proposed to be the possible active species, especially for the catalytic systems in which the temperatures are required higher than 750 °C [15,16]. Superoxide species $O^{2-\bullet}$* anion radicals were also observed on the surfaces of the catalysts such as LaOF [17], Ba/Nd_2O_3 [18], and Y_2O_3-CaO [19]. Moreover, it was known that the reactivity of $O^{2-\bullet}$* increased with the rise of the temperature [20]. Osada *et al.* were able to show that $O^{2-\bullet}$* species could be stable up to 1023 K to react with CH_4 over Y_2O_3-CaO catalysts [19]. Given the mechanistic information above, it is unsurprising that the rational

* Corresponding author.
E-mail address: xmcao@ecust.edu.cn (X.-M. Cao).

http://dx.doi.org/10.1016/j.cclet.2020.09.015
1001-8417/

design for the catalyst focuses on the activation of methane by modulating the formation of the suitable reactive oxygen species [7].

For the methane oxidation, Yang *et al.* found that the local hot pot, which was easy to be formed during the methane oxidation, would result in the deep oxidation of methane towards CO_2 [21]. Hence, the thermal conductivity should be an important characteristic for the promising materials catalyzing methane partial oxidation. Thus, as a typical two-dimensional (2D) material, the hexagonal boron nitride (*h*-BN) sheet, exhibiting the superb thermal stability (up to 1000 K) and high thermal conductivity [22–24], would be a good matrix for methane oxidation. Metal subnanoclusters supported on the 2D material have been found to exhibit an unusually high activity for CO electrooxidation [25], enabling them to be attractive candidates for the next generation catalysts. Recent theoretical studies suggested that single metal atoms such as Au, Cu, and Fe embedded in graphene or *h*-BN also possess the high performance for oxygen activation [26–30]. Different from the formidable O_2 activation on the pristine *h*-BN [31], it was found that the O_2 could be activated by the metal doped graphene or *h*-BN nanosheets with the strong adsorption energy and the stretched O—O bond. Moreover, the binding of oxygen on the TM-BNs was stronger than the corresponding M-graphene [32]. The doped *h*-BN was therefore proved to enjoy the high activity for CO oxidation [31]. Yet it still remains elusive for the methane activation [33,34], which is sensitive to the kind of oxygen species. Two primary questions remain to be settled: (1) which kind of oxygen specie is formed when O_2 chemisorbs on the metal doped *h*-BN surface? (2) what kind of oxygen species could activate the C–H bond of methane?

In this work, we computationally investigated the oxidative dehydrogenation of CH_4 on a series of single transition metal (TM) atom from group 4–11 embedded defective *h*-BN monolayer based on the density functional theory (DFT) calculations. It has been reported that the single point defect vacancy, such as B-vacancy and N-vacancy, could be formed during the growth of BN nanosheet or be produced by solvent exfoliation [35,36]. Since the boron vacancy (B-vac) has been proved to be more stable than the nitrogen vacancy (N-vac) by both experiment and theory [37], the stability and reactivity for methane oxidative dehydrogenation of TM-BNs would be systematically investigated based on the single TM atom anchored on the boron monovacancy. The relationship between the kind of formed oxygen species and the embedded metal cation was firstly explored and analyzed. The competition between the direct C–H bond activation and O_2 adsorption was also compared. Then, the reactivities of formed surface oxygen species for the first C–H bond activation were computationally investigated. Finally, we proposed some possible rules to promote the methane activation through choosing the kind of embedded metal atom.

The single-layer *h*-BN utilizing a 12.540 Å × 15.047 Å × 15.000 Å was selected and a single metal atom was embedded in the energetically favourable B-vacancy. All the calculations were carried out using Vienna Ab-initio Simulation Package (VASP) [38–40] with the projector augmented wave method and a cutoff energy of 500 eV. The generalized gradient approximation method was chosen with Perdew-Burke-Ernzerhof (PBE) functional for the exchange-correlation term [41] (see details in the Supporting information).

As the examples of group 6 TM-BNs, the TM atom lies above the *h*-BN plane with three equivalent M–N bonds (Fig. S1 in Supporting information). It could be found from Table 1 that the M–N length exhibits the regular variation. The M–N lengths are always greater than 1.90 Å for 4d and 5d TM atoms, while they are shorter than 1.90 Å for 3d TM atoms. Interestingly, different from the variation of the atomic radius of TMs, the M–N length from left to right across the periodic table gradually decreases firstly but rallies after group 9. The Ag-N bond is the longest M–N bond with a length of 2.10 Å, while the Co-N bond is the shortest M–N bond with a length of 1.76 Å.

Table 1
The M–N bond distance (Å) for the TM–BN with the B-vacancy and the bader charge of embedded metal cation for TM atom at the B-vacancy.

TM-BN	M–N (Å)	Q(M)	TM–BN	M–N (Å)	Q (M)	TM-BN	M–N (Å)	Q (M)
Ti-BN	1.88	+1.35 e	Zr-BN	2.02	+1.41 e	Hf-BN	1.98	+1.41 e
V-BN	1.85	+1.31 e	Nb-BN	1.96	+1.48 e	Ta-BN	1.96	+1.36 e
Cr-BN	1.83	+1.28 e	Mo-BN	1.95	+1.23 e	W-BN	1.94	+1.28 e
Mn-BN	1.84	+1.25 e	Tc-BN	1.93	+1.07 e	Re-BN	1.93	+1.11 e
Fe-BN	1.77	+1.06 e	Ru-BN	1.92	+0.90 e	Os-BN	1.92	+0.94 e
Co-BN	1.76	+0.94 e	Rh-BN	1.91	+0.79 e	Ir-BN	1.91	+0.81 e
Ni-BN	1.79	+0.91 e	Pd-BN	1.99	+0.73 e	Pt-BN	1.97	+0.70 e
Cu-BN	1.83	+0.92 e	Ag-BN	2.10	+0.73 e	Au-BN	2.06	+0.67 e

To evaluate the stability of the TM-BNs, the binding energies of the TM atom at the B-vacancy with reference to its bulk were investigated. As shown in Fig. S2 (Supporting information), all the binding energies are negative, indicating that the TM-BNs could be prepared and steadily exist rather than the clustering. This is in agreement with the experimental results that the doped TM at the B vacancy of *h*-BN could be easily achieved without the clustering effect [42,43]. Moreover, among all the TM-BNs, the Ti has the strongest binding energy of -5.86 eV while the weakest binding energy is the metal Au. For the same group, the binding strength generally follows the order: 3d > 4d > 5d. It indicates that the 3d TM atom is easier to be embedded. In the same period, the stability gradually decreases from right to the left across the periodic table. The charge of TM atom exhibits the similar trend (Table 1). The positive Bader charges of all the atomic TMs indicate that the atomic TMs are cations and the significant electron transfer from the atomic TM to the coordinated N atoms. The spin states of metal atoms also indicate the electron transfer (Table S1 in Supporting information). Importantly, in the same period, the atomic TM gradually becomes less positive from right to the left across the periodic table. It indicates that the stability of the atomic TMs associates with the charge transfer process.

The O_2 could not be chemisorbed on the *h*-BN, in which the O—O bond still keeps at 1.208 Å which is the same as that of gaseous O_2 (Fig. S3 in Supporting information). On the contrary, it could be strongly bound with TM-BNs. It prefers to be chemisorbed on the single TM center of TM-BNs *via* the π mode (Fig. 1). All the adsorption energies are negative and rather strong. Except for the group 11, the adsorption energies are more negative than -1.00 eV (Fig. S4 in Supporting information). Moreover, the O—O bond has been stretched to longer than 1.30 Å by TM-BNs. The strong adsorption energy and stretched O—O bond suggest that the O_2 is activated by the TM center. In addition, the negative charge of O_2

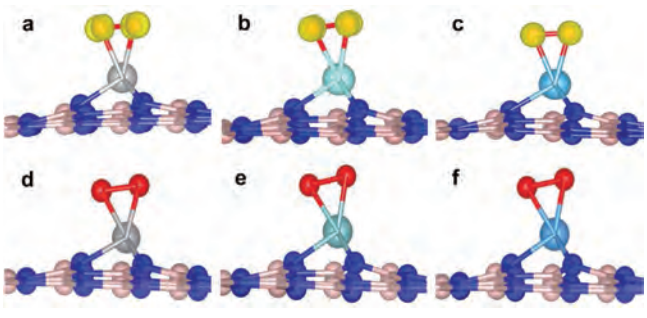

Fig. 1. The spin density map of O_2* adsorbed on the TM-BN: (a) Ti-BN, (b) Zr-BN, (c) Hf-BN, (d) V-BN, (e) Nb-BN and (f) Ta-BN. Color scheme: B, pink; N, dark blue; O, red.

implies the significant electron transfer from the TM atom to the O_2 during its chemisorption (Table S2 in Supporting information).

Intriguingly, the adsorption strength of O_2 in different periods follows the order of 5d > 4d > 3d in the same group (Fig. S4 in Supporting information), which is opposite to the stability of TM center at TM-BN. From right to left across the periodic table in the same period, the adsorption strength firstly climbs upward to reach the maxima at group 5 followed by the monotonic decrease. Consequently, the adsorption strength of O_2 reaches the maxima at Ta-BN with the extremely strong adsorption energy of -6.07 eV.

The spin density was further mapped for the O_2^* (The asterisk denotes the surface species) over 24 TM-BNs. The specific data of spin states are shown in Table S3 in Supporting information. Interestingly, it is found that the TM-BNs could be classified into two types, corresponding to two kinds of formed O_2 species: TM-BN(I): The superoxide ($O^{2-\bullet *}$) could be formed over the TM-BNs, including the TM atoms in the groups 4, 9, 10 and 11 besides Ir; TM-BN(II): The peroxide (O_2^{2-*}) could be formed over the TM-BNs, including the TM atoms in groups 5, 6, 7 and 8, and Ir. The spin density of O_2^* over the TM-BNs of groups 4 and 5 are respectively taken as the examples of two types (Fig. 1). Notably, a spin electron is left in O_2^* over the TM-BNs of group 4, while no spin electron exists in O_2^* over the TM-BNs of group 5. Furthermore, comparing the lengths of O_2^*, we could find that the O—O bond of O_2^* over the TM-BNs(I) is shorter than 1.40 Å, exhibiting the superoxide-like character. On the contrary, the O—O bond of O_2^* is longer than 1.40 Å over the TM-BNs(II), exhibiting the peroxo-like character (Fig. S5 in Supporting information). It is consistent with the previously reported results of $O^{2-\bullet *}$ and O_2^{2-*} [12,44,45].

The origin to the formation of two kinds of O_2^* species could be attributed to the number of the valence electron of TM center and the work function of TM-BN. As displayed in Fig. S6 (Supporting information), from left to right across the periodic table, the work function of TM-BNs generally keeps increasing growth, indicating that TM-BNs become more difficult to lose the electrons. This explains why $O^{2-\bullet *}$ instead of O_2^{2-*} could be formed on the TM-BNs with the TM atoms located in the groups on the right side. Moreover, it is worth noting that for TM in group 4 has only four valence electrons. This indicates that it can only lose one electron to O_2 when three M–N bonds are formed. Consequently, $O^{2-\bullet *}$ rather than O_2^{2-*} would also form on the TM-BNs of group 4. Hence, O_2^{2-*} could only be formed over the TM-BNs in the middle groups with enough valence electrons and lower work function.

For the C–H bond activation of CH_4 under the oxidizing condition, it could occur *via* either direct dehydrogenation by the TM-BNs or oxidative dehydrogenation by the reactive surface oxygen species. We firstly check the possibility of the direct dehydrogenation. The first C–H bond could be activated by the TM center of TM-BN to yield coadsorbed CH_3^* and H^* (Fig. S7 in Supporting information). Its dissociation energy is plotted in Fig. 2a. It could be found that the variation trend of the C–H bond dissociation energy is analogical to the adsorption energy of O_2. Comparing different periods, the released energy after the first C–H bond dissociation follows the order of 5d > 4d > 3d. From right to left across the same period, the dissociation energy firstly becomes more exothermic from group 4–5 and then gradually turns more endothermic. Consequently, Ta-BN also exhibits the best performance for the first C–H bond breaking. However, comparing the O_2 adsorption and the C–H bond activation, it is obvious that the O_2 adsorption always releases more heat. Hence, the O_2 would preferentially occupy the TM center of the TM-BNs rather than the CH_3^* and H^* from CH_4 dissociation during oxidation process. Hence, the first C–H bond activation has to be triggered *via* the oxidative dehydrogenation by O_2^*.

For the oxidative dehydrogenation by O_2^*, the C–H bond activation has to be triggered *via* the radical mechanism without the direct help from the TM center to produce the gaseous $CH_3^{\bullet}$ radical and the bounded H at the O since the TM center has been occupied by O_2^*.

Interestingly, different from direct dehydrogenation, group 6 outperforms group 5 for CH_4 oxidative dehydrogenation by O_2^*. As displayed in Fig. 2b, for 3d TM, the TM-BN is always difficult to launch CH_4 oxidative dehydrogenation. For 4d and 5d TM, from right to left across the same period, the oxidative dehydrogenation firstly becomes more favorable thermodynamically from group 4 to group 6 and then gradually turns more unfavorable. Moreover, in the same group, 5d TM-BN is always more favorable than 4d TM-BN for CH_4 oxidative dehydrogenation. Consequently, W-BN exhibits the best performance for the first C–H bond oxidative dehydrogenation.

Importantly, associating the oxidative dehydrogenation product and the reaction energies with the kind of O_2^* species, we can find that two kinds of O_2^* species could significantly affect the formed surface intermediates. As two typical examples of Ti-BN and Ta-BN displayed in Fig. S8 (Supporting information), after breaking the first C–H bond, the O^* and OH^* could be formed from peroxide O_2^{2-*} except those on Cr-BN, Mn-BN and Fe-BN, while OOH^* could be generally formed from the superoxide $O^{2-\bullet *}$ as well as the peroxide O_2^{2-*} on Cr-BN, Mn-BN and Fe-BN. Since the reactivity of O_2^* is regulated by the TM-BNs, the TM center would modulate the activity of the C–H bond activation indirectly.

Comparing their reaction energies, it is clear from Fig. 2b that the formation of OOH^* is considerably endothermic, requiring the energy at least higher than 1.46 eV. This indicates that CH_4 is not easy to be activated by the TM-BNs(I) with the formation of superoxide species and Cr-BN, Mn-BN and Fe-BN under the mild conditions. This is mainly due to the fact that the formation of

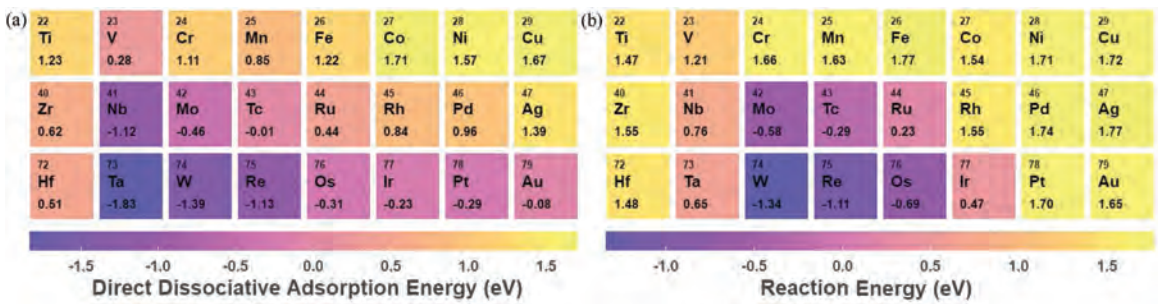

Fig. 2. (a) The map for the CH_4 direct dissociative adsorption energy (eV) on TM-BNs. (b) The map of reaction energies (eV) for the first step of CH_4 oxidative dehydrogenation to form gaseous $CH_3^{\bullet}$ on TM-BNs.

O—H bonding in OOH* is unable to compensate the loss of the C–H bond dissociation of CH_4. On the other hand, on the TM-BNs(II) except Cr-BN, Mn-BN and Fe-BN, the C–H bond breaking with the assistance of superoxide O^{2-}* is evidently less endothermic than those over the TM-BNs(I). Except for Ti-BN, the reaction energies are all lower than 1.00 eV. Especially on Mo-BN, Tc-BN, W-BN, Re-BN, and Os-BN, the reaction turns to be exothermic. It indicates that peroxide species can activate the C–H bond of methane more easily than superoxide. This might mainly originate from the strong oxophilicity of these TMs for the formation of strong M–O bonding to compensate the loss of C–H and O—O bonds breaking.

Interestingly, several linear relationships could be found between the reaction energy of the oxidative dehydrogenation of CH_4 and the length of O—O bond (Fig. 3A). Notably, these linear relationships are sensitive to the kind of O_2* species. For the reaction triggered by the superoxide, the reaction energy is well linearly related to the O—O bond length of O^{2-}*. For those triggered by the peroxide species, three different linear relationships could be found. Accordingly, the TM-BNs(II) could be divided into three categories: TM-BNs(II-a): Cr-, Mn- and Fe-BNs; TM-BNs (II-b): group 5 including V-, Nb- and Ta-BNs; TM-BNs(II-c): Mo-, Tc-, Ru-, W-, Re-, Os-, and Ir-BNs.

Since OOH* rather than O* and OH* is produced on the TM-BNs (II-a), it stands to reason that TM-BNs(II-a) would not be located in the same line of the other TM-BNs for the reaction energy against the O—O bond length. To gain a deeper understanding on the origin to these different linear relationships, the spin densities of the surface oxygen species on the TM-BNs(II) after CH_4 oxidative dehydrogenation were mapped. The specific spin states are listed in Table S4 (Supporting information). The Nb-, Mo-, Tc-, Ta-, W- and Re-BNs are taken as the examples displayed in Fig. 3B. On the Nb- and Ta-BNs of group 5, O* has a single electron spin while no spin exists at OH* and TM, indicating that O^{-}* radical and OH^{-}* are produced. On the Mo^{-} and W-BNs of group 6, no spin electron is detected, indicating that O^{2-}* and OH^{-}* are produced. On the Tc- and Re-BNs of group 7, no spin is located at the O species but a single electron spin is left at the TM. Hence, on the TM-BNs of group 5, the formation of less stable O^{-}* radical leads to the highly endothermic process of CH_4 oxidative dehydrogenation and the resulting new line curve.

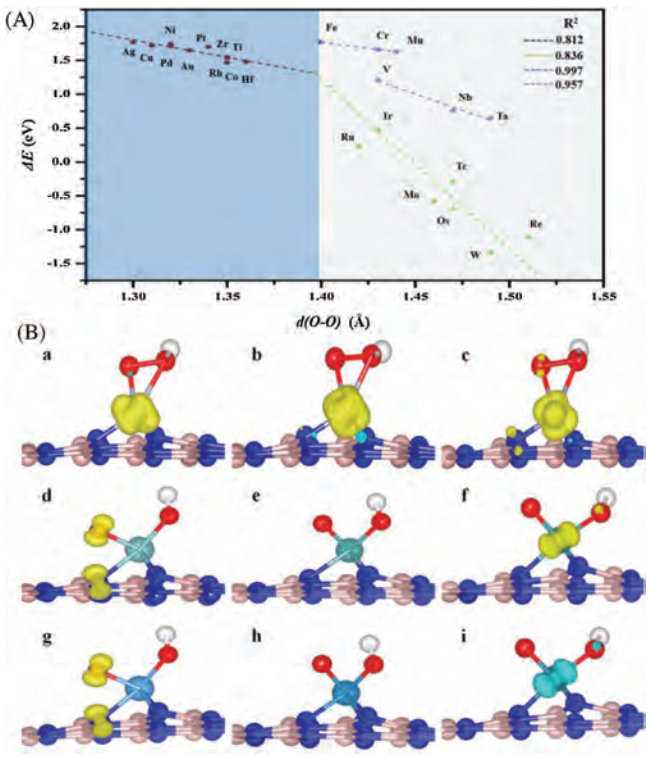

Fig. 3. (A) The reaction energy for the first C—H bond activation against the O—O bond length. The O—O bond length of 1.40 Å is the boundary to distinguish the kind of O_2* species. (B) The spin density map of the surface oxygen containing intermediates after the first C—H activation of methane by O_2* on the (a) Cr-BN, (b) Mn-BN, (c) Fe-BN, (d) Nb-BN, (e) Mo-BN, (f) Tc-BN, (g) Ta-BN, (h) W—BN and (i) Re-BN; Color scheme: H, white; B, pink; N, dark blue; O, red.

Similar to the origin to the formation of superoxide and peroxide, the number of valence electrons would also be responsible for the formation of O^{-}* or O^{2-}*. For the formation of O^{2-}* and OH^{-}* on TM-BNs, the TM atom has to offer extra three electrons besides the three electrons for the formation of three M–N bonds. Hence, only the TMs in group 5 and the groups on its right, which possess more than six valence electrons, could provide enough electrons to guarantee the formation of O^{2-}* and OH^{-}*. Moreover, with the increase of the work function from right to left across the periodic table, the TM cations become difficult to lose electrons. Consequently, the oxidative dehydrogenation of CH_4 by O_2* is easy to occur over the TM-BNs of group 6. O^{-}* and OH^{-}* are possible to be formed on the

TM-BNs of group 5. In addition, the Bronsted-Evans-Polanyi relationship could be found for the oxidative dehydrogenation of CH_4 by O_2* to produce O* and OH* (Fig. S9 in Supporting information). These TM-BNs with the reaction energies of CH_4 oxidative dehydrogenation lower than 0.80 eV are possible candidates to activate CH_4. Last but not least, we further checked the possibility of O^{-}* and O^{2-}* from peroxide to activate CH_4. As listed in Table S5 (Supporting information), the oxidative dehydrogenation of CH_4 catalyzed by O^{2-}* over TM-BNs(II-c) is dramatically endothermic, requiring the energy high than 2.00 eV. This indicates that O^{2-}* is inert to activate CH_4. For the O^{-}* over Nb-BN and Ta-BN, although the reaction is still endothermic, the energy barriers for the C–H bond breaking are around 0.70 eV, indicating that O^{-}* is able to activate CH_4 at the mild condition. Nevertheless, for the whole CH_4 oxidation, although O^{-}* is unable to activate CH_4 dehydrogenation, it is possible to trigger the other steps such as the C—O coupling with gaseous $CH_3^{\bullet}$. These steps are beyond the scope of the work. We would not further discuss them.

On the basis of the above discussions, we can find that superoxide is difficult to activate CH_4 over TM-BNs under the mild conditions. When O* and OH* are possible to be produced, peroxide species could activate the C–H bond of CH_4. Although the generation of O^{-}* through the H abstraction from CH_4 by $O_2{}^{2-}$* over Nb-BN and Ta-BN is more difficult than the O^{2-}* over the TM-BNs(II-c), O^{-}* is remarkably more active to abstract H from CH_4 than O^{2-}*. $O_2{}^{2-}$* and O^{-}* are possible surface reactive oxygen species for CH_4 oxidative dehydrogenation on the TM-BNs. For TM-BNs catalysts, $O_2{}^{2-}$* over W-BN is the most active O_2 species to launch the first C–H bond activation of CH_4, while the possibly formed O^{-}* over Nb- and Ta-BNs is also reactive for methane activation. Importantly, the calculation results unveil that the electronic structures of oxygen species strongly depend on the valence electron number of TM atom and its work function influenced by their coordination environment. Hence, the optimum single TM center for TM-BNs may not be suitable for the other single atom catalysts for methane activation.

Based on the systematic investigation on the first C–H bond activation of methane over TM-BNs, we could find that most of the TMs could be strongly bound at the boron monovacancy of *h*-BN monolayer. 3d TMs embedded in the boron monovacancy of *h*-BN exhibit higher stability than 4d or 5d TMs. Moreover, the stability of single atomic TM gradually decreases from right to the left across the periodic table in the same period.

Although TMs are bound at the defect strongly, O_2 could still strongly chemisorb on these single TM centers and be activated. After the chemisorption of O_2, the superoxide $O^{2-\bullet}$* could be formed over the TM-BNs including the TM atoms in the groups 4, 9, 10 and 11 besides Ir, while the peroxide ${O_2}^{2-}$* could be formed over the TM-BNs including the TM atoms of groups 5, 6, 7 and 8, and Ir. The binding strength of O_2 follows the order of 5d > 4d > 3d for TM-BNs in the same group. Group 5 exhibits the maximum adsorption strength for O_2. The electronic structure of ${O_2}^*$ is determined by the valence electron number and the coordination environment of the TM center and the work function of TM-BN.

O_2 adsorption is thermodynamically far more favorable than CH_4 direct dissociative adsorption at single TM center. Consequently, CH_4 activation must rely on the oxidative dehydrogenation by reactive surface oxygen species. The electronic structure of surface oxygen species on TM-BN determines the activity of methane oxidative dehydrogenation. Superoxide $O^{2-\bullet}$* is difficult to activate CH_4 while those peroxide ${O_2}^{2-}$*, which could form O^{2-}* after CH_4 oxidative dehydrogenation, would trigger the first C–H bond activation of CH_4 easily. However, the produced O^{2-}* is unable to catalyze the CH_4 dehydrogenation. On the Ta-BN and Nb-BN, the formed peroxide ${O_2}^{2-}$* is likely to activate CH_4 as well and the formed $O^{-\bullet}$* after the first step oxidative dehydrogenation is very reactive to launch the further CH_4 oxidative dehydrogenation. The underlying reason for the formation of different oxygen species and the resulting activity for CH_4 oxidative dehydrogenation is the redox potential of TM center, including its valence electron number, coordination environment, and the work function of TM-BN. These electronic properties are related to the electronic structure of *h*-BN.

Declaration of competing interest

The authors report no declarations of interest.

Acknowledgments

The authors gratefully acknowledge the financial support from the National Natural Science Foundation of China (NSFC, Nos. 21673072 and 91845111), Program of Shanghai Subject Chief Scientist (No. 17XD1401400), Shanghai Science and Technology Committee (No. 17520750100) and the Fundamental Research Funds for the Central Universities.

Appendix A. Supplementary data

Supplementary material related to this article can be found, in the online version, at doi:https://doi.org/10.1016/j.cclet.2020.09.015.

References

[1] P. Tang, Q. Zhu, Z. Wu, D. Ma, Energy Environ. Sci. 7 (2014) 2580–2591.
[2] C. Mesters, Annu. Rev. Chem. Biomol. Eng. 7 (2016) 223–238.
[3] H. Schwarz, Angew. Chem. Int. Ed. 50 (2011) 10096–10115.
[4] S.J. Blanksby, G.B. Ellison, Acc. Chem. Res. 36 (2003) 255–263.
[5] C. Hammond, S. Conrad, I. Hermans, ChemSusChem 5 (2012) 1668–1686.
[6] J.A. Labinger, ChemInform 220 (2004) 27–35.
[7] R. Horn, R. Schlögl, Catal. Lett. 145 (2015) 23–39.
[8] W. Hu, J. Lan, Y. Guo, X.M. Cao, P. Hu, ACS Catal. 6 (2016) 5508–5519.
[9] Y. Lou, J. Ma, W. Hu, et al., ACS Catal. 6 (2016) 8127–8139.
[10] W. Hu, X.M. Cao, P. Hu, J. Phys. Chem. C 122 (2018) 19593–19602.
[11] W. Hu, Z.J. Shao, X.M. Cao, P. Hu, Chin. J. Catal. 41 (2020) 1369–1377.
[12] M.S. Palmer, M. Neurock, M.M. Olken, J. Am. Chem. Soc. 124 (2002) 8452–8461.
[13] V.J. Ferreira, P. Tavares, J.L. Figueiredo, J.L. Faria, Ind. Eng. Chem. Res. 51 (2012) 10535–10541.
[14] J.H. Lunsford, Catal. Today 6 (1990) 235.
[15] M.Y. Sinev, V.N. Korchak, O.V. Krylov, Kinet. Catal. 27 (1987) 1110–1112.
[16] D. Dissanayake, J.H. Lunsford, M.P. Rosynek, J. Catal. 143 (1993) 286–298.
[17] W. Weng, M. Chen, H. Wan, Y. Liao, Catal. Lett. 53 (1998) 42–50.
[18] C.T.A. Peter, Y.W. Liu, C.F. Ng, J. Catal. 176 (1998) 365–375.
[19] Y. Osada, S. Koike, T. Fukushima, S. Ogasawara, Appl. Catal. 59 (1990) 59–74.
[20] M. Iwamoto, J.H. Lunsford, J. Phys. Chem. 84 (1980) 3079–3084.
[21] Z. Liu, Y. Yang, ACS Catal. 8 (2018) 11761–11772.
[22] C.R. Dean, A.F. Young, I. Meric, et al., Nat. Nanotechnol. 5 (2010) 722–726.
[23] K. Watanabe, T. Taniguchi, H. Kanda, Nat. Mater. 3 (2004) 404–409.
[24] C.Y. Zhi, Y. Bando, C.C. Tang, H. Kuwahara, D. Golberg, Adv. Mater. 21 (2009) 2889–2893.
[25] E. Yoo, T. Okata, T. Akita, Nano Lett. 9 (2009) 2255–2259.
[26] Y. Li, Z. Zhou, G. Yu, J. Phys. Chem. C 114 (2010) 6250–6254.
[27] E.H. Song, Z. Wen, Q. Jiang, J. Phys. Chem. C 115 (2011) 3678–3683.
[28] Y.H. Lu, M. Zhou, C. Zhang, J. Phys. Chem. C 113 (2009) 20156–20160.
[29] M. Gao, A. Lyalin, T. Taketsugu, J. Phys. Chem. C 116 (2012) 9054–9062.
[30] S. Lin, X. Ye, R.S. Johnson, H.J. Guo, J. Phys. Chem. C 117 (2013) 17319–17326.
[31] Y. Wang, L. Zhao, L. Shi, et al., Catal. Sci. Technol. 8 (2018) 2051–2055.
[32] C. Huang, X. Ye, C. Chen, S. Lin, D. Xie, Comput. Theor. Chem. 1011 (2013) 5–10.
[33] J. Xu, X.M. Cao, P. Hu, J. Phys. Chem. C 123 (2019) 28802–28810.
[34] Y. Wang, L. Zhao, X.M. Cao, et al., Catal. Sci. Technol. 8 (2018) 2051–2055.
[35] W. Sun, Y. Meng, Q. Fu, ACS Appl. Mater. Interfaces 8 (2016) 9881–9888.
[36] J. Zhao, Z. Chen, J. Am. Chem. Soc. 139 (2017) 12480–12487.
[37] C. Jin, F. Lin, K. Suenaga, Phys. Rev. Lett. 102 (2009) 195505.
[38] G. Kresse, J. Furthmuller, Comp. Mater. Sci. 6 (1996) 15–50.
[39] G. Kresse, J. Hafner, Phys. Rev. B 49 (1994) 14251.
[40] G. Kresse, J. Furthmüller, Phys. Rev. B 54 (1996) 11169–11186.
[41] J.P. Perdew, K. Burke, M. Ernzerhof, Phys. Rev. Lett. 77 (1996) 3865–3868.
[42] B. Huang, H. Xiang, J. Yu, S.H. Wei, Phys. Rev. Lett. 108 (2012) 206802.
[43] Y.G. Zhou, P. Yang, F. Gao, et al., Phys. Chem. Chem. Phys. 13 (2011) 7378–7383.
[44] Q. Meng, W. Wang, X. Weng, et al., J. Phys. Chem. C 120 (2016) 3259–3266.
[45] J. Wang, G.C. Wang, J. Phys. Chem. C 122 (2018) 17338–17346.